Optimizing Performance of Silicon-Based p−n Junction Photodetectors by the Piezo-Phototronic Effect
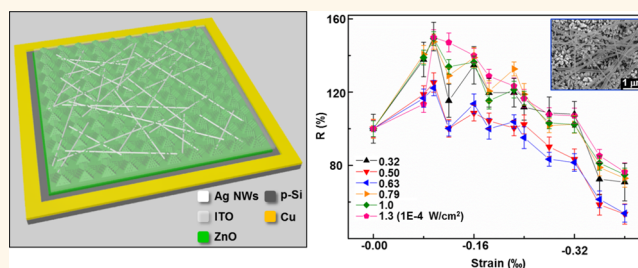
Zhaona Wang,[†,‡,#] Ruomeng Yu,[†,#] Xiaonan Wen,[†,#] Ying Liu,[†] Caofeng Pan,[§] Wenzhuo Wu,[†] and Zhong Lin Wang*,[†,§]

[†]School of Materials Science and Engineering, Georgia Institute of Technology, Atlanta, Georgia 30332-0245, United States, [‡]Department of Physics, Beijing Normal University, Beijing, China, 100875, and [§]Beijing Institute of Nanoenergy and Nanosystems, Chinese Academy of Sciences, Beijing, China, 100083. [#]Z. Wang, R. Yu, and X. Wen contributed equally to this work.

ABSTRACT Silicon-based p−n junction photodetectors (PDs) play an essential role in optoelectronic applications for photosensing due to their outstanding compatibility with well-developed integrated circuit technology. The piezo-phototronic effect, a three-way coupling effect among semiconductor properties, piezoelectric polarizations, and photon excitation, has been demonstrated as an effective approach to tune/modulate the generation, separation, and recombination of photogenerated electron−hole pairs during

optoelectronic processes in piezoelectric-semiconductor materials. Here, we utilize the strain-induced piezo-polarization charges in a piezoelectric n-ZnO layer to modulate the optoelectronic process initiated in a p-Si layer and thus optimize the performances of p-Si/ZnO NWs hybridized photodetectors for visible sensing *via* tuning the transport property of charge carriers across the Si/ZnO heterojunction interface. The maximum photoresponsivity R of 7.1 A/W and fastest rising time of 101 ms were obtained from these PDs when applying an external compressive strain of −0.10‰ on the ZnO NWs, corresponding to relative enhancement of 177% in R and shortening to 87% in response time, respectively. These results indicate a promising method to enhance/optimize the performances of non-piezoelectric semiconductor material (*e.g.*, Si) based optoelectronic devices by the piezo-phototronic effect.

KEYWORDS: piezo-phototronic effect · p−n junction · photodetector · silicon-based

Silicon-based optoelectronic devices have become increasingly important and played a profound role in information and communication technologies in the era of "systems-on-a-chip"[1] due to their excellent compatibility with well-developed integrated circuit technology. Combining with the rapidly developed nanotechnologies in semiconductor materials, plenty of silicon-based nano/microscale optoelectronic components, such as photodetectors (PDs),[2,3] light-emission diodes,[1,4] and lasers,[5] have been extensively investigated during the last decades. Among which, ultrasensitive PDs featuring fast response time and miniaturized device size are opening possible opportunities to integrated optoelectronic systems for various applications, such as laser-related sensor networks, optical communications, and many more.[6] However, most of the reported silicon-based nano/micro-PDs are still suffering

from difficulties of further improving the photoresponsivity and lacking of adjustability.[7−10]

The piezo-phototronic effect, a three-way coupling effect among semiconductor properties, piezoelectric polarizations, and photoexcitations, has been demonstrated as an effective approach to tune/modulate the generation, separation, and recombination of electron−hole pairs during optoelectronic processes.[11,12] Significant enhancements on the performance of solar cells,[13,14] light emission diodes,[11,12,15,16] and photodetectors[17−19] have been achieved by modulating the charge carrier transport, separation, or recombination across the local junction/interface through strain-induced piezoelectric polarization charges. Although the piezo-phototronic effect has been reported to be effective in improving the performances of piezoelectric semiconductor materials-based optoelectronics,
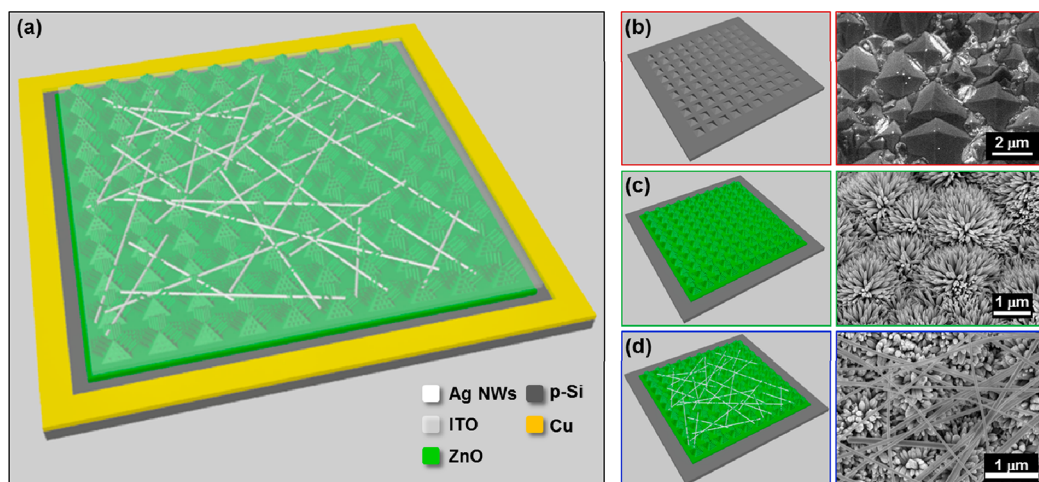
Figure 1. Device fabrication. (a) Schematic structure of a p-Si/n-ZnO NW hybridized PD. (b−d) Schematic structure (left panel) and SEM images (right panel) of (b) etched Si wafer and p-Si/n-ZnO heterojunctions (c) before and (d) after spin coating Ag NWs.

it has not been investigated yet for silicon-based electronic/optoelectronic devices.

Here we designed and fabricated a p-Si/ZnO nanowire (NW) hybridized PD by utilizing strain-induced piezo-polarization charges on the piezoelectric n-ZnO side to modulate the optoelectronic process initiated on the p-Si side and thus optimize the performance of a photosensing device. Experimental results indicate that silicon-based ZnO NW hybridized PDs can effectively respond to visible-range optical signals. The general performances of the PD are optimized and significantly enhanced after introducing a piezo-phototronics effect[11,20] by externally applying strains to modify the interface properties at the Si/ZnO heterojunction. Under a compressive strain of −0.10‰, a photoresponsivity R of 7.1 A/W was obtained, corresponding to an enhancement factor of 177%; the fastest rising time of 101 ms was achieved with 87% improvement. The optimal performances are attributed to the strain-induced piezo-polarization charges at the Si/ZnO heterojunction interface, where the generation, separation, and recombination of electron−hole pairs are modulated through the modifications of the depletion region and band structures. These results indicate the capability of the piezo-phototronic effect to effectively enhance/optimize the performances of silicon-based optoelectronic devices.

RESULTS AND DISCUSSION

The structure of an as-fabricated p−n junction PD is schematically illustrated in Figure 1a. A textured p-type Si wafer with micropyramids 2−4 μm in size (Figure 1b) is produced by etching a Si wafer[21] to increase the surface area for better light absorption. The obtained Si micropyramid structure is then covered by a thin layer of ZnO as a seed layer and ZnO nanowires as an antireflection coating to improve the energy-conversion efficiency,[18,22] forming p-Si/n-ZnO

heterojunctions with highly dense ZnO NWs grown perpendicular to the surface of Si micropyramids along the c-axis direction as shown in Figure 1c. To increase the conductivity of the top electrode, Ag nanowires are dispersed on a ZnO NW array as shown in Figure 1d. Finally, the ITO layer and copper are sputtered on the ZnO NW array and the p-type Si as the transparent top electrode and the bottom electrode, respectively. Detailed fabrication procedures are described step by step in the Methods section.

The output signals of p-Si/n-ZnO NWs hybridized PDs under different external strain conditions and without any illumination were first measured and plotted in Figure 2a. The amount of strain applied to the ZnO NWs is estimated based on Young's modulus ratio among different materials by assuming a uniform distribution of forces among each layer of the device for the state of mechanical equilibrium;[12] tensile strain is defined as positive and compressive strains as negative (Methods). The stronger the externally applied strain, the higher the output current, as shown in I−V characteristics of the p−n heterojunction PDs. The inset of Figure 2a indicates a near-linear increase of output current from 20 μA (strain-free) to more than 155 μA (−0.32‰ strain) when the bottom electrode (p-Si) is biased at 2 V. Significantly, the rectifying performance of the p-Si/n-ZnO heterojunction is obviously enhanced, indicated by the rectification ratio I_F/I_R (I_F and I_R stand for the forward and reverse currents, respectively)[23] increasing from 8 to 63. Therefore, by simply applying external strains, the interface properties of the p−n heterojunction are improved.

On the basis of a 2D physical model using real dimensions of a p-Si/n-ZnO NW hybridized structure as parameters (Methods), a finite element analysis is conducted to simulate the strain/piezoelectric potential distributions in ZnO NW arrays, as shown in Figure 2b. When pressing the device with a force of
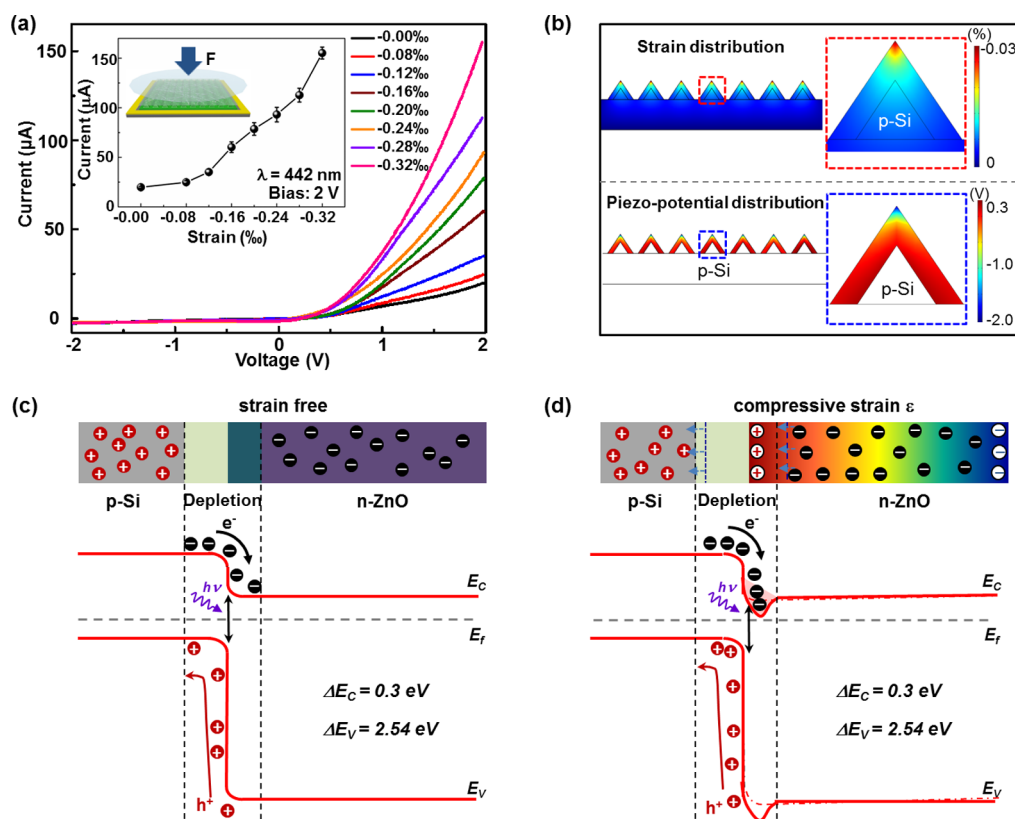
Figure 2. Working mechanism. (a) $I-V$ characteristics of the device under different strain conditions without laser illumination. The inset shows the current changes with the external strains when a 2 V bias is applied. (b) Simulation results of strain distribution (top panel) and piezoelectronic potential distribution (bottom panel) in the ZnO nanowire array by FEA. (c, d) Schematic band diagrams of a p-Si/n-ZnO heterojunction (c) without and (d) with compressive strain applied to illustrate the working mechanism of piezo-phototronic effect optimized p−n junction PDs.

10 N, the simulation results clearly show that the compressive strain mainly distributes in ZnO NWs near the tips of the micropyramids (top panel in Figure 2b). The corresponding piezo-potential distributions are also illustrated in color codes, as shown in Figure 2b (bottom panel), by knowing the polarity of the external strains (compressive) and the crystalline orientation of the ZnO NWs (c-axis pointing outward perpendicular to the surface of micropyramid Si).[11] The positive piezo-potential distributes at the local interface of the n-ZnO/p-type Si heterojunction, effectively modulating the separation process of light-generated electron−hole pairs by tuning the energy band structure of the piezoelectric ZnO NWs array. The negative piezo-potential distributes at the tip of the micropyramid, where ZnO NWs form contacts with the ITO top electrode; this is equivalent to applying an additional forward bias voltage on the PD. Thus, the output current increases when applying more compressive strain, as shown by the $I-V$ characteristics in Figure 2a.

The influence of compressive strain on the photo-generated carriers' transport process at the p-Si/n-ZnO interface is understood from the expansion of the depletion width on the p-Si side[15] and the modification of the band diagram based on Anderson's model[24] (Figure 2c,d). The band gap and electron affinity values for Si and ZnO are $E_{g,Si}$ = 1.12 eV,[24] χ_{Si} = 4.05 eV[24] and $E_{g,ZnO}$ = 3.36 eV, χ_{ZnO} = 4.35 eV,[25] respectively. Once a p−n heterojunction is formed, a conductive band offset ΔE_c = 0.3 eV and a valence band offset ΔE_v = 2.54 eV[23] are present at the local interface, as shown in Figure 2c. Upon visible light (442 nm) illumination, photons pass through the n-ZnO layer and are mostly absorbed in the underlying p-Si considering the band gaps of both materials, generating electron−hole pairs and thus increasing the output current. Under compressive strain, the depletion width on the p-Si side is increased by positive piezo-polarization charges present at local interface of the p-Si/n-ZnO heterojunction.[15] The depletion region expands and shifts toward the p-Si side[15] because of the presence of positive piezoelectric charges at the junction. This expansion of the depletion region on the p-Si side will effectively increase the photon-absorption volume and thus lead to a larger amount of charge carriers generated under illumination especially for visible light that mostly generates the electron−hole carriers on the Si side. On the other hand, the positive piezo-polarization charges displayed at the p−n heterojunction interface on the n-ZnO side also attract and trap some of the photogenerated electrons, which is equivalent to forming a dip at both conduction and
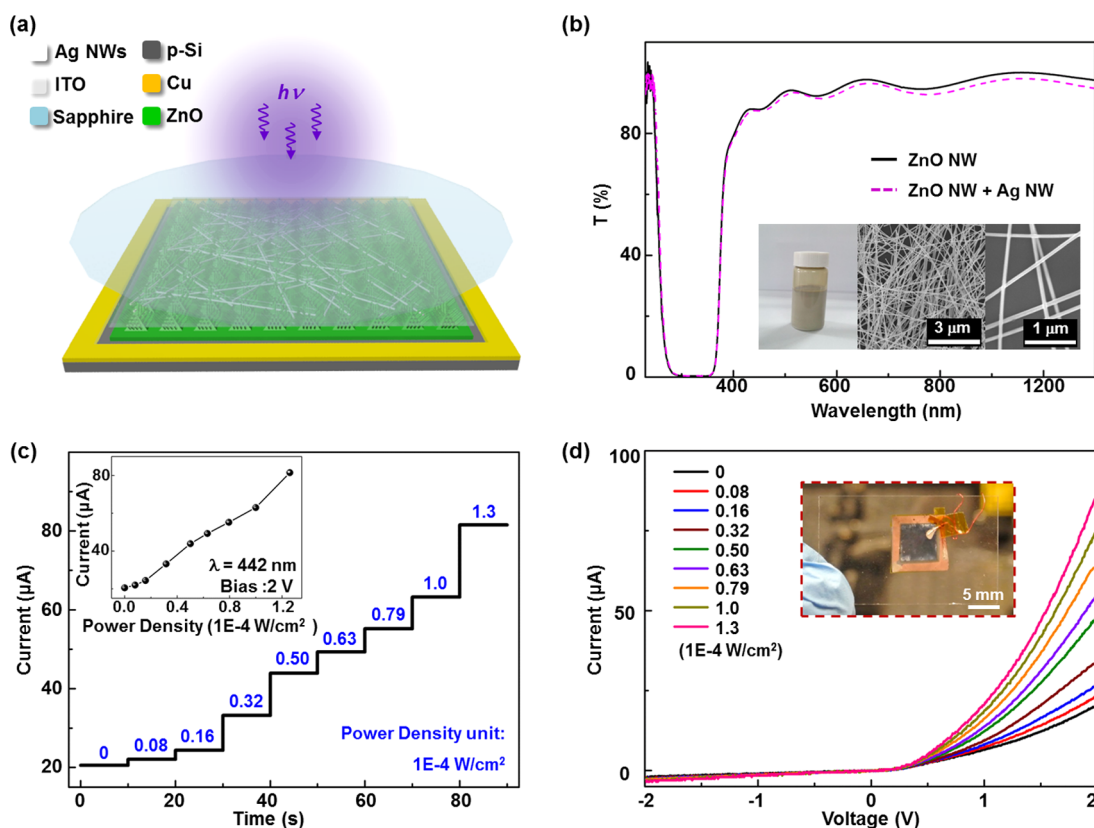
C

Figure 3. General photoresponse of p-Si/n-ZnO NWs hybridized PDs. (a) Schematic illustration of the experimental setup. (b) Transmission spectra of a ZnO NWs array on the glass (black solid line) and the ZnO NWs coated with Ag NWs (purple dashed line). The insets are a photograph and SEM images of Ag NWs. (c) $I-t$ response of the device under different illumination power densities at 2 V bias voltage. The inset shows the current change with the power density. (d) $I-V$ characteristics of the device under different illumination power densities when a triangle wave is applied. The inset shows a photograph of the real device.

valence bands of ZnO NWs (Figure 2d). This trapping mechanism retards the effective separation of photogenerated electron−hole pairs and therefore reduces the photocurrent. The two above-described processes will compete with the increase of strain; thus, there exists an optimum strain at which the performance of the PD is maximized. Our experimental results will show such a result. This is the fundamental working principle of piezo-phototronic effect optimized performance of p-Si/n-ZnO hybridized visible PDs.

The general photon-response performance of p-Si/n-ZnO NWs hybridized PDs is carefully investigated and summarized in Figure 3 by applying 442 nm laser illumination (Figure 3a). The transmission spectra of ZnO NWs synthesized on a glass substrate (black solid line) under the same growing conditions as those on a p-Si and ZnO NWs array covered by Ag NWs (purple dashed line) are presented in Figure 3b, together with a photograph and SEM images of Ag NWs as insets. It is obvious that both ZnO and Ag NWs are almost transparent to the 442 nm lasing ($T \approx 90\%$), indicating the photogeneration process happens mostly on the p-Si side at the local junction/interface. Fixing the forward bias voltage at 2.0 V, the light response of p-Si/n-ZnO NWs hybridized PDs under 442 nm laser illumination to nine different power densities ranging from 0 to

1.3×10^{-4} W/cm^2 is presented in Figure 3c. The output current increased from 20.5 μA (dark current), through 43.9 μA (5×10^{-5} W/cm^2), to 81.5 μA (1.3×10^{-4} W/cm^2). The inset current vs power density plot clearly shows a linear relationship between the output current and the power density, facilitating the calibration for practical applications. By applying a triangular wave across the device, the corresponding $I-V$ characteristics are also presented in Figure 3d together with a photograph of the real device.

Piezo-phototronic effect optimized performances of p-Si/n-ZnO NWs hybridized PDs are systematically investigated by applying a series of light power densities as well as external strains to the devices. The output currents of the PDs are measured and summarized in Figures 4a and S1a (Supporting Information) by applying a fixed bias voltage of 2 V across the p−n junction. Under each power density (from 3.2×10^{-5} to 1.3×10^{-4} W/cm^2), 11 different strains ranging from −0.00‰ to −0.40‰ are exerted onto the PD to measure its optoelectronic behavior, indicating an obvious increase in output currents by increasing either the light power density or the external strains. The photocurrent $\Delta I = I - I_{\text{dark,s}}$ ($I_{\text{dark,s}}$ represents the corresponding dark current under certain strains) are calculated and presented in Figure 4b, clearly showing that, under each
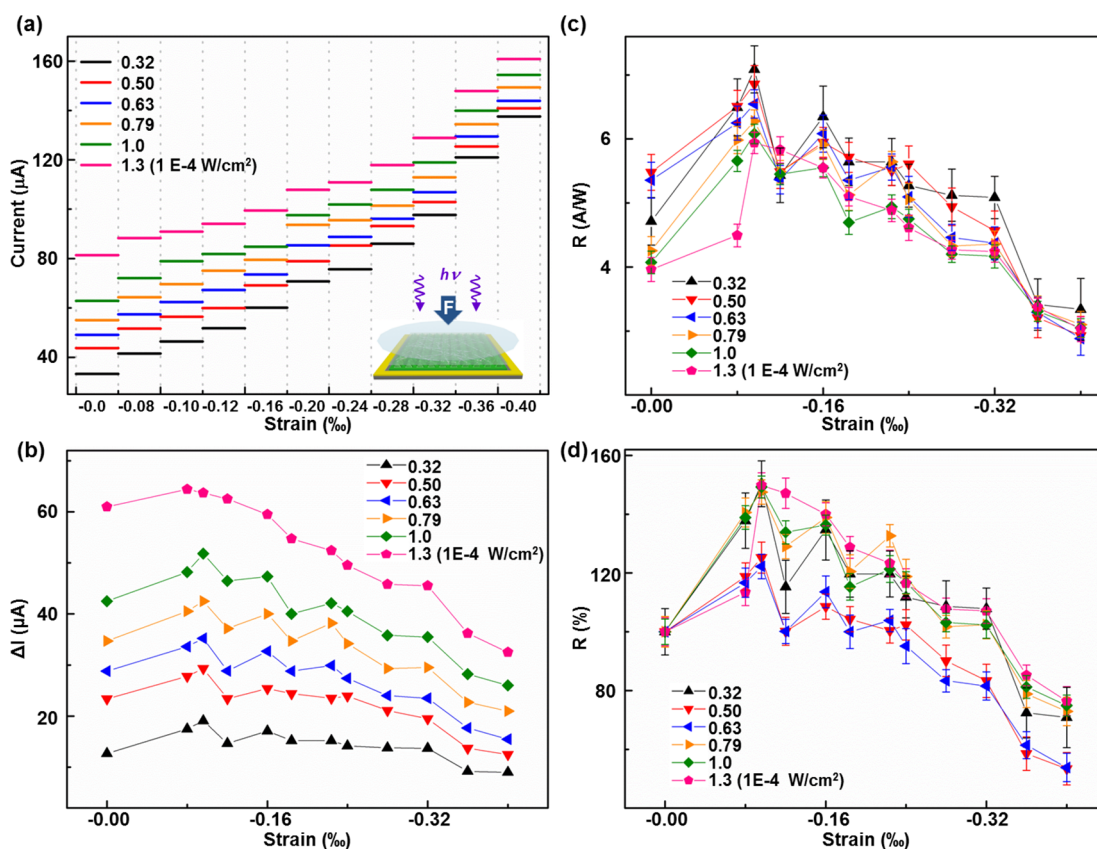
Figure 4. Piezo-phototronic effect. (a) Output current of the PDs under different strain and illumination conditions at 2 V bias voltage. The inset shows a schematic illustration of the experimental setup. (b) Photocurrent, (c) photoresponsivity, and (d) relative changes of photoresponsivity of the device under different strain and illumination conditions, biased at 2 V.

strain condition, the photocurrent increases with an increase in the power density of illumination. Moreover, a local maximum value of photocurrent ΔI is obtained at $-0.10‰$ compressive strain under illuminations with power densities from 3.2×10^{-5} to 1.3×10^{-4} W/cm^2, indicating the optimization of PD performances by the piezo-phototronic effect.

As a critical parameter of PDs, the photoresponsivity R is also calculated as shown in Figure 4c for all the power densities and external strain conditions with the bottom electrode 2 V biased. The photoresponsivity[26] R is defined as

$$R = \frac{I_{\text{light, s}} - I_{\text{dark, s}}}{P_{\text{ill}}} = \frac{\eta_{\text{ext}} q}{h\nu} \Gamma_G$$

where $P_{\text{ill}} = I_{\text{ill}} \times S$ is the illumination power on the PD; $I_{\text{light,s}}$ and $I_{\text{dark,s}}$ represent the photon and dark current under the corresponding external strain, respectively; Γ_G is the internal gain; η_{ext} is the external quantum efficiency (EQE); q is the electronic charge; h is Planck's constant; ν is the frequency of the light; I_{ill} is the excitation power density; S is the effective area of the PD. A maximum value of R is obviously concluded from Figure 4c under each power density, with the highest value of 7.1 A/W under $-0.10‰$ strain at a power density of 3.2×10^{-5} W/cm^2, corresponding to a relative enhancement of 177%. This achieved R value

is larger than that of a commercial Si photodiode PD (in the range $0.1-0.2$ A/W at 442 nm),[27] near 100 times larger in magnitude than that obtained from a Si/ZnO core−shell NW array PD (1.0×10^{-2} A/W, 480 nm, -1 V),[28] also larger than that of a Si/CdS core−shell NW network PD (<1 A/W, 480 nm, -1 V).[29]

To illustrate the piezo-phototronics effect on photoresponsivity more clearly, relative changes of photoresponsivity R with respect to R_0 (corresponding photoresponsivity at no strain) are calculated and summarized in Figure 4d. It is observed that, under each power density, the relative change of R varyies with applied strain in a similar manner to that of photocurrent ΔI (Figure 4b) and photoreponsivity R (Figure 4c), displaying a maximum value at an external strain of $-0.10‰$. In addition, the specific detectivity D^* is also calculated as

$$D^* = R/(2e \cdot I_{\text{dark, s}}/S)^{0.5}$$

where $I_{\text{dark,s}}$ is the dark current under the corresponding external strain (considered as the major noise) and S is the surface area of PD.[30] Figure S1b (Supporting Information) presents the highest detectivity D^* of 7.1×10^9 Jones with an applied external strain of $-0.10‰$ under each incident light power density. The maximum value derived in photocurrent,
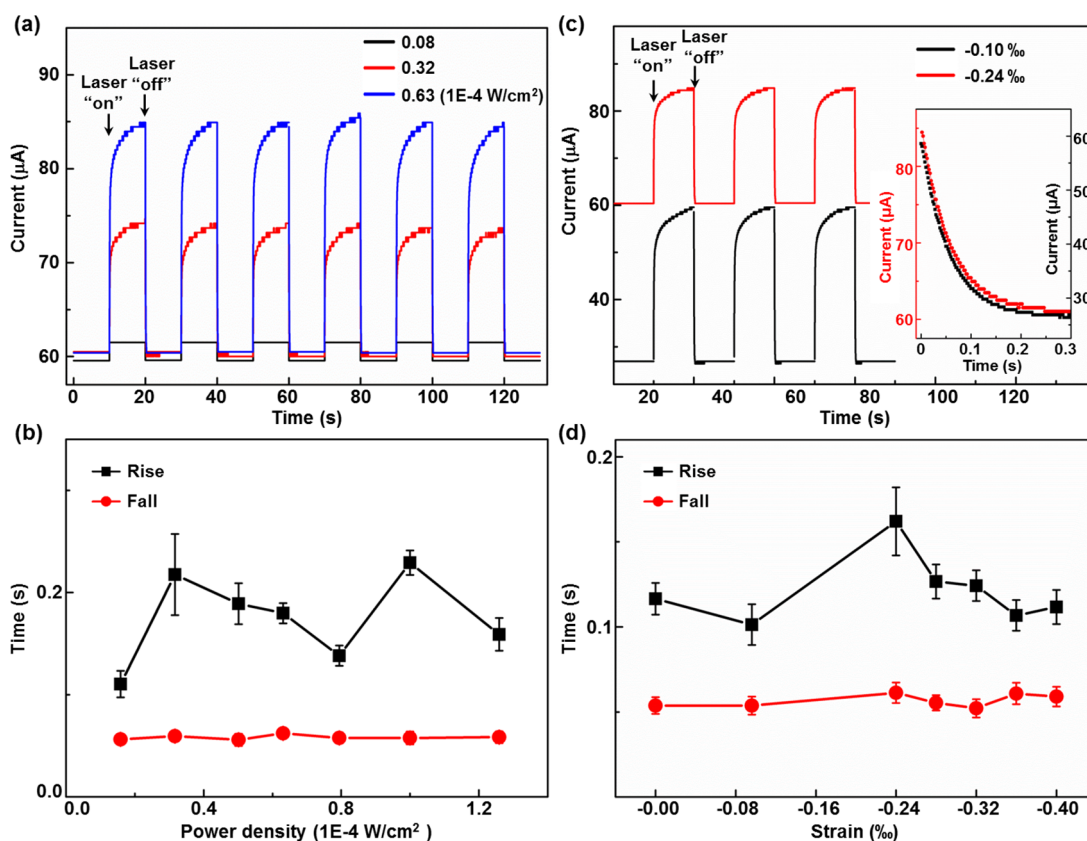
Figure 5. Repeatability and time response of the PDs. (a) Repeatability and time response and (b) the corresponding rise and fall time of the device under different illumination power densities, under −0.24‰ external strains. (c) Repeatability and time response and (d) the corresponding rise and fall time of the device under different compressive strains, under a power density of 6.3 × 10⁻⁵ W/cm².

photoresponsivity, relative change of *R*, and the detectivity *D** is attributed to the simultaneously existing competition between the expansion of the depletion region in p-Si and the trapping mechanism of the photogenerated carriers as a dip in energy band of n-ZnO upon straining.

The stability and repeatability of the p-Si/n-ZnO NW hybridized PDs are presented in Figure 5a by switching the 442 nm laser source under 8.0×10^{-6}, 3.2×10^{-5}, and 6.3×10^{-5} W/cm² for six repeated cycles. The output current presents impressive consistency and repeatability for all illumination conditions. To clearly show the changes of response time at rise/fall edges with the power density, a weight-averaged rise time and fall time[31] of the PD are calculated from the *I*−*t* curve under 2 V forward bias and presented in Figure 5b based on the best fit double-exponential function.[31,32] A short fall time of the PD fluctuating near 57 ms and relative long rise time ranging from 110 to 229 ms are obtained. A similar measurement is carried out and presented in Figure 5c by applying different strains to the device illuminated by a 442 nm laser under a power density of 6.3×10^{-5} W/cm². Following the same fitting approach described above, weight-averaged rise time and fall time are calculated and shown in Figure 5d under different external strains.

No significant changes of the fall time are observed when various strains are applied to the p-Si/n-ZnO NW hybridized PD, which can be seen clearly from enlarged fall edges as the inset in Figure 5c, while a minimum value of 101 ms is observed for the rise time at an external strain of −0.10‰, corresponding to a relative change of 87%.

CONCLUSIONS

In summary, the piezo-phototronic effect is utilized to modulate the optoelectronic behaviors of the non-piezoelectric semiconductor material and thus to optimize the performances of silicon-based p−n junction visible photosensing devices. Upon applying strain, piezoelectric polarization charges are induced at the local interface to effectively modulate the band structure and the depletion width of the p-Si/n-ZnO heterojunction. The coexisting expansion of the depletion region in p-Si and the trapping mechanism in n-ZnO contribute to the optimal performances of PDs by controlling the transport properties of charge carriers across the local p−n junction. The maximum photoresponsivity *R* of 7.1 A/W and fastest rising time of 101 ms are obtained from these PDs when applying an external compressive strain of −0.10‰ on the ZnO NWs, corresponding to a relative enhancement of

177% in *R* and shortening to 87% in response time, respectively. This work provides a potential approach to enhance/optimize the performances of silicon-based optoelectronic devices by the piezo-phototronic effect.

METHODS

Device Fabrication Process. In our experiment, the p-type silicon wafer (B doped (100) wafer, 1−30 Ωcm, University Wafer) is etched by KOH at 85 °C for 30 min.[21] The etching solution is composed of KOH (2.0 wt %), deionized (DI) water, and isopropyl alcohol (5.0 vol %). The obtained Si wafer with micropyramids is then ultrasonically cleaned for 2 min in acetone, distilled water, and ethanol, consecutively. Next, a 100 nm ZnO seed layer is deposited on silicon by radio frequency (RF) magnetron sputtering at room temperature (PVD75 system, Kurt J. Lesker Company). The coated silicon wafers are then placed into the mixed nutrient solutions (0.02 mM $Zn(NO_3)_2$ and 0.02 mM HMTA) for ZnO NWS growth *via* a hydrothermal method in a mechanical convection oven (Yamato model DKN400, Santa Clara, CA, USA) at 85 °C for 1 h. In order to get separated ZnO NWs, 0−5 mL of ammonium hydroxide (Sigma-Aldrich) is added per 100 mL of mixing solution. After cooling the whole system, the product was washed with ethanol and DI water, collected, and vacuum-dried. A thin layer of Ag NWs is spin coated onto the ZnO-covered silicon for better conductivity. Finally, thin layers of ITO (100 nm) and copper (200 nm) are deposited as the transparent top electrode and the bottom electrode by RF magnetron sputtering at room temperature (PVD75 system), respectively. Testing wires are connected to the top and bottom electrodes by silver paste. The active area of the device is 8 mm × 8 mm.

Materials Characterization. Detailed microscopic structures of pyramid nanostructures of p-type Si, ZnO, and Ag NWs are characterized by scanning electron microscope (SEM) (Hitachi SU8010).

External Strain Calculations. External strains are applied onto the p-Si/n-ZnO PD by pressing the surface of the device through a piece of sapphire with a 3D mechanical stage (movement resolution ~10 μm), while fixing the device on a manipulation holder through two layers of double-sided Kapton polyimide tape with a thickness of 100 μm (consisting of 25 μm Kapton film and a 75 μm silicone adhesive layer). Considering the Young's modulus of silicone is 0.001 GPa (obtained from the manufacturer), which is much smaller than that of other materials (Kapton ~2.5 GPa, Si ~150 GPa, ZnO ~129 GPa) stacked in the device, when applying a certain compressive force on the system, most of the deformation is produced in the silicone layers. Under the condition of static mechanic equilibrium, the forces are uniformly distributed in different layers of materials, and then the strain in ZnO NWs is calculated based on the Young's modulus ratio among these materials.[12] The strain value corresponds to the longitudinal strain along the *c*-axis of ZnO NWs with tensile strain defined as positive and compressive strain as negative.

Measurement. Transmission spectra of ZnO and ZnO/Ag NWs are measured by a UV−visible spectrophotometer (JΛSCO V-630). *I*−*V* characteristics of the device are measured and recorded by a computer-controlled measurement system with a Stanford SRS low noise current preamplifier (SR570)/SRS low noise voltage preamplifier (SR560) in conjunction with a GPIB controller (GPIB-USB-HS, NI 488.2). The optical input stimuli are provide by a He−Cd laser (wavelength = 442 nm, model no. KI5751I-G, Kimmon Koha Co., Ltd.). A continuously variable filter is used to control the light power density, which is measured by a thermopile powermeter (Newport 818P-001-12). An objective is used to expand the 442 nm laser beam. The diameter of the laser beam illuminated on the device is 4 mm.

Theoretical Simulation. A two-dimensional physical model using real dimensions of p-Si/n-ZnO NWs hybridized PDs as parameters is employed for finite element analysis to simulate the strains and piezoelectric potential distributions within ZnO NWs arrays upon straining by simplifying the ZnO NWs to a film coated on the pyramid structures. The simulation parameters are as follows: the bottom side length and the height of the micropyramids are 2 and 1.7 μm (Figure 2b), respectively. The thickness of the ZnO film is about 1 μm (Figure 2b and c). The ITO electrode layers with a thickness of 100 nm are ignored in this calculation. The *c*-axis of the ZnO layer is pointing outward perpendicular to the surface of the micropyramids. Material constants of ZnO used in this calculation are the same as those in our previous report.[33] The Young's modulus, Poisson ratio, and density of the Si are E = 150 GPa, ν_P = 0.17, and ρ = 2.33 × 10^3 kg/m^3, respectively. A compression force of 10 N is applied to this model by pressing the p−n junction PD. All calculations are carried out by using the COMSOL package.

Conflict of Interest: The authors declare no competing financial interest.

Supporting Information Available: More detailed information about *I*-strain characteristics and the detectivity *D** change with the external strain of p-Si/n-ZnO NW hybridized visible PDs under a series of power density and external strain conditions. This material is available free of charge *via* the Internet at http://pubs.acs.org.

REFERENCES AND NOTES

1. Hirschman, K. D.; Tsybeskov, L.; Duttagupta, S. P.; Fauchet, P. M. Silicon-Based Visible Light-Emitting Devices Integrated into Microelectronic Circuits. *Nature* **1996**, *384*, 338–341.
2. Hayden, O.; Agarwal, R.; Lieber, C. M. Nanoscale Avalanche Photodiodes for Highly Sensitive and Spatially Resolved Photon Detection. *Nat. Mater.* **2006**, *5*, 352–356.
3. Michel, J.; Liu, J. F.; Kimerling, L. C. High-Performance Ge-on-Si Photodetectors. *Nat. Photonics* **2010**, *4*, 527–534.
4. Huh, C.; Kim, K. H.; Kim, B. K.; Kim, W.; Ko, H.; Choi, C. J.; Sung, G. Y. Enhancement in Light Emission Efficiency of a Silicon Nanocrystal Light-Emitting Diode by Multiple-Luminescent Structures. *Adv. Mater.* **2010**, *22*, 5058–5062.
5. Rong, H. S.; Xu, S. B.; Kuo, Y. H.; Sih, V.; Cohen, O.; Raday, O.; Paniccia, M. Low-Threshold Continuous-Wave Raman Silicon Laser. *Nat. Photonics* **2007**, *1*, 232–237.
6. Lee, S. Y.; Park, K. I.; Huh, C.; Koo, M.; Yoo, H. G.; Kim, S.; Ah, C. S.; Sung, G. Y.; Lee, K. J. Water-Resistant Flexible GaN LED on a Liquid Crystal Polymer Substrate for Implantable Biomedical Applications. *Nano Energy* **2012**, *1*, 145–151.
7. Guo, Z.; Zhao, D. X.; Liu, Y. C.; Shen, D. Z.; Zhang, J. Y.; Li, B. H. Visible and Ultraviolet Light Alternative Photodetector Based on ZnO Nanowire/n-Si Heterojunction. *Appl. Phys. Lett.* **2008**, *93*, 163501.
8. Ismail, R. A.; Al-Naimi, A.; Al-Ani, A. A. Studies on Fabrication and Characterization of a High-Performance Al-Doped ZnO/n-Si (111) Heterojunction Photodetector. *Semicond. Sci. Technol.* **2008**, *23*, 075030.
9. Zhang, T. C.; Guo, Y.; Mei, Z. X.; Gu, C. Z.; Du, X. L. Visible-Blind Ultraviolet Photodetector Based on Double Heterojunction of n-ZnO/Insulator-MgO/p-Si. *Appl. Phys. Lett.* **2009**, *94*, 113508.
10. Liu, C. C.; Hu, S. L.; Shen, S. P. Effect of Flexoelectricity on Electrostatic Potential in a Bent Piezoelectric Nanowire. *Smart Mater. Struct.* **2012**, *21*, 115024.
11. Wang, Z. L. Progress in Piezotronics and Piezo-Phototronics. *Adv. Mater.* **2012**, *24*, 4632–4646.
12. Pan, C. F.; Dong, L.; Zhu, G.; Niu, S. M.; Yu, R. M.; Yang, Q.; Liu, Y.; Wang, Z. L. High-Resolution Electroluminescent

Imaging of Pressure Distribution Using a Piezoelectric Nanowire LED Array. *Nat. Photonics* **2013**, *7*, 752–758.

13. Wen, X. N.; Wu, W. Z.; Wang, Z. L. Effective Piezo-Phototronic Enhancement of Solar Cell Performance by Tuning Material Properties. *Nano Energy* **2013**, *2*, 1093–1100.

14. Pan, C. F.; Niu, S. M.; Ding, Y.; Dong, L.; Yu, R. M.; Liu, Y.; Zhu, G.; Wang, Z. L. Enhanced Cu_2S/CdS Coaxial Nanowire Solar Cells by Piezo-Phototronic Effect. *Nano Lett.* **2012**, *12*, 3302–3307.

15. Liu, Y.; Niu, S.; Yang, Q.; Klein, B. D.; Zhou, Y. S.; Wang, Z. L. Theoretical Study of Piezo-Phototronic Nano-LEDs. *Adv. Mater.* **2014**, *26*, 7209–7216.

16. Yang, Q.; Liu, Y.; Pan, C. F.; Chen, J.; Wen, X. N.; Wang, Z. L. Largely Enhanced Efficiency in ZnO Nanowire/p-Polymer Hybridized Inorganic/Organic Ultraviolet Light-Emitting Diode by Piezo-Phototronic Effect. *Nano Lett.* **2013**, *13*, 607–613.

17. Yang, Q.; Guo, X.; Wang, W. H.; Zhang, Y.; Xu, S.; Lien, D. H.; Wang, Z. L. Enhancing Sensitivity of a Single ZnO Micro-/Nanowire Photodetector by Piezo-phototronic Effect. *ACS Nano* **2010**, *4*, 6285–6291.

18. Zhang, F.; Niu, S. M.; Guo, W. X.; Zhu, G.; Liu, Y.; Zhang, X. L.; Wang, Z. L. Piezo-Phototronic Effect Enhanced Visible/UV Photodetector of a Carbon-Fiber/ZnO-CdS Double-Shell Microwire. *ACS Nano* **2013**, *7*, 4537–4544.

19. Yu, R. M.; Pan, C. F.; Hu, Y. F.; Li, L.; Liu, H. F.; Liu, W.; Chua, S.; Chi, D. Z.; Wang, Z. L. Enhanced Performance of GaN Nanobelt-Based Photodetectors by Means of Piezotronic Effects. *Nano Res.* **2013**, *6*, 758–766.

20. Wang, Z. L. Piezopotential Gated Nanowire Devices: Piezotronics and Piezo-Phototronics. *Nano Today* **2010**, *5*, 540–552.

21. Yang, Y.; Zhang, H. L.; Chen, J.; Lee, S. M.; Hou, T. C.; Wang, Z. L. Simultaneously Harvesting Mechanical and Chemical Energies by a Hybrid Cell for Self-Powered Biosensors and Personal Electronics. *Energy Environ. Sci.* **2013**, *6*, 1744–1749.

22. Liu, Y.; Das, A.; Xu, S.; Lin, Z. Y.; Xu, C.; Wang, Z. L.; Rohatgi, A.; Wong, C. P. Hybridizing ZnO Nanowires with Micropyramid Silicon Wafers as Superhydrophobic High-Efficiency Solar Cells. *Adv. Energy Mater.* **2012**, *2*, 47–51.

23. Dutta, M.; Basak, D. P-ZnO/n-Si Heterojunction: Sol-gel Fabrication, Photoresponse Properties, and Transport Mechanism. *Appl. Phys. Lett.* **2008**, *92*, 212112.

24. Sze, S. M. Physics of Semiconductor-Devices. *CC/Eng. Tech. Appl. Sci.* **1982**, 28–28.

25. Aranovich, J. A.; Golmayo, D.; Fahrenbruch, A. L.; Bube, R. H. Photo-Voltaic Properties of ZnO-CdTe Heterojunctions Prepared by Spray Pyrolysis. *J. Appl. Phys.* **1980**, *51*, 4260–4268.

26. Konstantatos, G.; Sargent, E. H. Nanostructured Materials for Photon Detection. *Nat. Nanotechnol.* **2010**, *5*, 391–400.

27. Kasap, S. O. *Optoelectronics and Photonics: Principles and Practices*; Prentice Hall: NJ, 2001; p 37.

28. Sun, K.; Jing, Y.; Park, N.; Li, C.; Bando, Y.; Wang, D. L. Solution Synthesis of Large-Scale, High-Sensitivity ZnO/Si Hierarchical Nanoheterostructure Photodetectors. *J. Am. Chem. Soc.* **2010**, *132*, 15465–15467.

29. Manna, S.; Das, S.; Mondal, S. P.; Singha, R.; Ray, S. K. High Efficiency Si/CdS Radial Nanowire Heterojunction Photodetectors Using Etched Si Nanowire Templates. *J. Phys. Chem. C* **2012**, *116*, 7126–7133.

30. Liu, X.; Gu, L. L.; Zhang, Q. P.; Wu, J. Y.; Long, Y. Z.; Fan, Z. Y. All-Printable Band-Edge Modulated ZnO Nanowire Photodetectors with Ultra-High Detectivity. *Nat. Commun.* **2014**, *5*, 4007.

31. Soci, C.; Zhang, A.; Xiang, B.; Dayeh, S. A.; Aplin, D. P. R.; Park, J.; Bao, X. Y.; Lo, Y. H.; Wang, D. ZnO Nanowire UV Photodetectors with High Internal Gain. *Nano Lett.* **2007**, *7*, 1003–1009.

32. Ni, P. N.; Shan, C. X.; Wang, S. P.; Liu, X. Y.; Shen, D. Z. Self-Powered Spectrum-Selective Photodetectors Fabricated from n-ZnO/p-NiO Core-Shell Nanowire Arrays. *J. Mater. Chem. C* **2013**, *1*, 4445–4449.

33. Gao, Y.; Wang, Z. L. Equilibrium Potential of Free Charge Carriers in a Bent Piezoelectric Semiconductive Nanowire. *Nano Lett.* **2009**, *9*, 1103–1110.